

Investigating the 95 GeV Higgs Boson Excesses within the I(1+2)HDM

AYOUB HMISSOU ^{1*}, STEFANO MORETTI ^{2,3†}, LARBI RAHILI ^{1‡}

¹Laboratory of Theoretical and High Energy Physics, Faculty of Science, Ibnou Zohr University, B.P 8106, Agadir, Morocco.

²Department of Physics & Astronomy, Uppsala University, Box 516, SE-751 20 Uppsala, Sweden.

³School of Physics & Astronomy, University of Southampton, Southampton, SO17 1BJ, United Kingdom.

Abstract

In this work, we explore how the 2-Higgs Doublet Model (2HDM) Type-I, extended by an inert doublet, can provide an explanation for the recently observed excesses at the Large Hadron Collider (LHC) in the $\gamma\gamma$ and $\tau^+\tau^-$ final states. Hence, by imposing theoretical constraints and experimental bounds on the model parameter space, our findings show that a light CP-even Higgs boson, h , with a mass around 95 GeV, can account for these anomalies. This result aligns with the excess in $b\bar{b}$ signatures reported in earlier data from the Large Electron-Positron (LEP) collider.

1 Introduction

Since the discovery of a Higgs boson at the LHC in July 2012 [1,2], several analyses of experimental data have reported intriguing anomalies that seem to deviate slightly from the predictions of the Standard Model (SM), such as but not exclusively, apparent lepton flavour universality violation in B -meson decays observed in the $b \rightarrow c\ell\nu$ transition [3,4], the unsettled anomalous magnetic moment of the muon [5] and an excess in Dark Matter (DM) searches [6,7], all suggesting potential new physics.

Recently, hints of a possible new spin-0 particle, with a mass around 95 GeV, have emerged in multiple independent experiments, such as LEP [8] in the $e^+e^- \rightarrow Z\phi(\rightarrow b\bar{b})$ production and decay process (with a 2.3σ local excess observed) and CMS [9,10] when looking for additional Higgs bosons decaying in the $\tau^+\tau^-$ channel (with local significance of 2.6σ). Additionally, at the same mass value, ATLAS and CMS reported an anomaly with a local significance of 1.7σ and 2.9σ , respectively, in the di-photon final state based on their full Run 2 data [11,12], with a signal strength of $\mu_{\gamma\gamma}^{\text{ATLAS}} = 0.18 \pm 0.1$ and $\mu_{\gamma\gamma}^{\text{CMS}} = 0.33_{-0.12}^{+0.19}$. These observations, while not yet definitive, have sparked significant theoretical and experimental interest, as they could well point to physics Beyond the SM (BSM), including extended Higgs sectors or other phenomena.

In literature, this issue has been addressed in many BSM extensions, such as the 2HDM [13–16], the 2HDM plus a real (N2HDM) [17–19] or complex (S2HDM) [20,21] singlet, the

*ayoub1hmissou@gmail.com

†stefano.moretti@physics.uu.se/s.moretti@soton.ac.uk

‡l.rahili@uiz.ac.ma/rahililarbi@gmail.com

Next-to-Minimal Supersymmetric SM (NMSSM) [22, 23] and other (pseudo)scalar extensions, some of which can explain all these anomalies simultaneously. In fact, there are solutions to the 95 GeV anomalies where a superposition of a CP-even and a CP-odd Higgs boson is also possible to achieve compliance with data, such as in Refs. [24, 25].

In our study, we investigate to what extent adding an inert doublet to the 2HDM can help address such intriguing anomalies. The resulting model, namely the I(1+2)HDM, is a special case of the 3-Higgs Doublet Models (3HDMs) that have been proposed initially by Ref. [26] as a simple extension to 2HDMs with the main purpose of addressing several problems of the latter, including flavour physics, Electro-Weak Symmetry Breaking (EWSB) and DM. Adopting a CP-conserving version of the I(1+2)HDM, which embeds one inert and two active Higgs doublets, we focus on Type-I Yukawa interactions, where all fermions couple to the same Higgs field. This version of the model lends itself well to analytical calculations, featuring a compact parameter space that current and future data can strongly constrain. Importantly, the loop effects of the embedded inert charged scalar bosons, χ^\pm , may alter the contributions of the corresponding active states, H^\pm , thereby enhancing or suppressing the di-photon decay rate. A key objective of this paper is to firmly accommodate, within the I(1+2)HDM framework, the most prominent of the aforementioned anomalies, i.e., the one in $\gamma\gamma$ final states—and to explore the parameter space that reproduces it.

The rest of this paper is organised as follows. In Section 2, we provide a concise description of the I(1+2)HDM, while Section 3 discusses the relevant theoretical and experimental constraints considered in our analysis. Section 4 details our numerical methodology for scanning the model’s parameter space, aiming to provide a coherent explanation for the three anomalies and to assess their impact on the remaining Higgs spectrum. In Section 5, we present our main results, and we conclude in Section 6.

2 I(1+2)HDM

The I(1+2)HDM consists of two active $SU(2)_L$ Higgs doublets with hypercharge $Y = 1$ and one inert doublet. Including an additional scalar doublet into the 2HDM has received extensive attention and is considered one of the most thoroughly investigated extensions of the 2HDM [27, 28]. The I(1+2)HDM features a discrete $\mathbb{Z}_2 \times \mathbb{Z}'_2$ symmetry, where the first factor corresponds to the inert-doublet \mathbb{Z}_2 , with only the field η transforming as $\eta \rightarrow -\eta$, while $\Phi_{1,2} \rightarrow \Phi_{1,2}$. Furthermore, a softly broken \mathbb{Z}'_2 symmetry is introduced for the Higgs doublets, where Φ_1 remains unchanged and Φ_2 is transformed to its negative, $\Phi_2 \rightarrow -\Phi_2$. This symmetry breaking proposed by the Paschos-Glashow-Weinberg theorem [29] is necessary to avoid the occurrence of Flavour Changing Neutral Currents (FCNCs) at tree level.

The most general scalar potential invariant under both the SM gauge group and the intro-

duced discrete symmetries can be expressed as follows:

$$\begin{aligned}
V(\Phi_1, \Phi_2, \eta) = & -\frac{1}{2} \{m_{11}^2 \Phi_1^\dagger \Phi_1 + m_{22}^2 \Phi_2^\dagger \Phi_2 + [m_{12}^2 \Phi_1^\dagger \Phi_2 + \text{h.c.}]\} + m_\eta^2 \eta^\dagger \eta \\
& + \frac{\rho_1}{2} (\Phi_1^\dagger \Phi_1)^2 + \frac{\rho_2}{2} (\Phi_2^\dagger \Phi_2)^2 + \rho_3 (\Phi_1^\dagger \Phi_1) (\Phi_2^\dagger \Phi_2) + \rho_4 (\Phi_1^\dagger \Phi_2) (\Phi_2^\dagger \Phi_1) \\
& + \frac{1}{2} [\rho_5 (\Phi_1^\dagger \Phi_2)^2 + \text{h.c.}] + \frac{\rho_\eta}{2} (\eta^\dagger \eta)^2 \rho_{1133} (\Phi_1^\dagger \Phi_1) (\eta^\dagger \eta) + \rho_{2233} (\Phi_2^\dagger \Phi_2) (\eta^\dagger \eta) \\
& + \rho_{1331} (\Phi_1^\dagger \eta) (\eta^\dagger \Phi_1) + \rho_{2332} (\Phi_2^\dagger \eta) (\eta^\dagger \Phi_2) + \frac{1}{2} [\rho_{1313} (\Phi_1^\dagger \eta)^2 + \text{h.c.}] \\
& + \frac{1}{2} [\rho_{2323} (\Phi_2^\dagger \eta)^2 + \text{h.c.}]. \tag{1}
\end{aligned}$$

Here, ρ_i represent the quartic coupling parameters, while m_η^2 , m_{11}^2 , m_{22}^2 , and m_{12}^2 are mass-squared terms. The values of m_{22}^2 and m_{12}^2 are determined by the conditions for minimising the potential, with all parameters required to be real in order to ensure CP-conservation.

For a region of parameter space where EWSB may occur, the minimisation of this potential gives

$$\Phi_1 = \begin{pmatrix} 0 \\ v_1/\sqrt{2} \end{pmatrix}, \quad \Phi_2 = \begin{pmatrix} 0 \\ v_2/\sqrt{2} \end{pmatrix}, \tag{2}$$

where v_1 and v_2 are Vacuum Expectation Values (VEVs) of the neutral component of each (pseudo)scalar doublet Φ_i , while the η scalar doublet remains inert due to the \mathbb{Z}_2 symmetry, which ensures that its constituent (pseudo)scalar states do not mix with those of Φ_1 and Φ_2 .

So that, with three complex scalar $SU(2)_L$ doublets, there are twelve fields:

$$\Phi_1 = \begin{pmatrix} \phi_1^\pm \\ (v_1 + \eta_1 + iz_1)/\sqrt{2} \end{pmatrix}, \quad \Phi_2 = \begin{pmatrix} \phi_2^\pm \\ (v_2 + \eta_2 + iz_2)/\sqrt{2} \end{pmatrix}, \quad \eta = \begin{pmatrix} \chi^\pm \\ (\chi + i\chi_a)/\sqrt{2} \end{pmatrix}. \tag{3}$$

Therefore, apart from the three fields that are used to provide mass to the weak gauge bosons (W^\pm and Z), the remaining nine fields are physical (pseudo)scalar states. Here, we distinguish between two independent spectra.

- The first one reflects the pure 2HDM Higgs spectrum that consists of two CP-even Higgs bosons, h and H , one CP-odd state A , and two charged Higgs bosons H^\pm . The corresponding mass terms of these particles are denoted as m_h , m_H (with $m_h < m_H$), m_A , and m_{H^\pm} , respectively, and can be expressed in terms of the parameters of the potential and VEVs. The mass-squared matrix of the CP-even scalar sector can be diagonalised through the angle α whereas both the CP-odd and charged sectors share the same mixing angle, defined by the ratio of the two VEVs of the active Higgs fields, $\tan \beta = v_2/v_1$. For more details, we refer the reader to Refs. [30, 31].
- In addition, the inert sector is made up by three (pseudo)scalar particles, χ , χ_a , and χ^\pm , with squared masses given by (here, $v^2 = v_1^2 + v_2^2 = (246 \text{ GeV})^2$)

$$\begin{aligned}
m_{\chi^\pm}^2 &= m_\eta^2 + \frac{1}{2} \rho_a v^2, \\
m_\chi^2 &= m_{\chi^\pm}^2 + \frac{1}{2} (\rho_b + \rho_c) v^2, \\
m_{\chi_a}^2 &= m_{\chi^\pm}^2 + \frac{1}{2} (\rho_b - \rho_c) v^2, \tag{4}
\end{aligned}$$

where a so-called ‘dark democracy’ approach has been adopted, making it possible to redefine the new couplings as follows:

$$\begin{aligned}\rho_a &\equiv \rho_{1133} = \rho_{2233}, \\ \rho_b &\equiv \rho_{1331} = \rho_{2332}, \\ \rho_c &\equiv \rho_{1313} = \rho_{2323}.\end{aligned}\tag{5}$$

Thus, we are left with 12 free parameters,

$$\Sigma = \{m_h, m_A, m_H, m_{H^\pm}, m_{12}^2, \tan\beta, \sin\alpha, m_\chi, m_{\chi_a}, m_{\chi^\pm}, m_\eta^2, \rho_\eta\},\tag{6}$$

which we use then to describe the Higgs sector of the I(1+2)HDM, while considering H as SM-like (i.e., $m_H \approx 125$ GeV).

Furthermore, following the enforcement of the symmetries described above, the most general Yukawa interactions in the I(1+2)HDM remain similar to those of the 2HDM and the corresponding Lagrangian reads as

$$\mathcal{L}_{\text{Yuk}}^{\text{I(1+2)HDM}} = -\bar{Q}_L Y_u \tilde{\Phi}_u u_R - \bar{Q}_L Y_d \Phi_d d_R - \bar{L}_L Y_\ell \Phi_\ell \ell_R + \text{h.c.} \supset - \sum_{f=u,d,\ell} \frac{m_f}{v} (\xi_h^f \bar{f} f h + \xi_H^f \bar{f} f H),\tag{7}$$

where Y_f ($f = u, d$ or l) are 3×3 Yukawa matrices and $\tilde{\Phi}_{1,2} = i\sigma_2 \Phi_{1,2}^*$, with $\sigma_{1,2}$ being the Pauli matrices. In Tab. 1 we list all the Type-I Yukawa couplings ξ_h^f and ξ_H^f of the CP-even Higgs bosons, h and H .

ξ_h^u	ξ_h^d	ξ_h^ℓ	ξ_H^u	ξ_H^d	ξ_H^ℓ
$\cos\alpha/\sin\beta$	$\cos\alpha/\sin\beta$	$\cos\alpha/\sin\beta$	$\sin\alpha/\sin\beta$	$\sin\alpha/\sin\beta$	$\sin\alpha/\sin\beta$

Table 1: Type-I Yukawa couplings of the neutral Higgs bosons h, H to the up-quarks, down-quarks and leptons in the I(1+2)HDM, normalised by the corresponding SM Yukawa couplings.

3 Theoretical and Experimental Constraints

For our randomly generated scan, we considered only points that are physically viable in the sense that they obey theoretical and experimental requirements. Here, we present a summary of the involved constraints imposed on the I(1+2)HDM Type-I.

3.1 Theoretical Constraints

These are the following ones.

- **Perturbativity:** We require that all quartic dimensionless couplings λ_i in Eq. (1) remain $\leq 8\pi$ to avoid a non-perturbative behaviour.
- **Unitarity:** To satisfy unitarity, it is necessary for the magnitudes of the eigenvalues of matrices, which are formed in the bases of different $2 \rightarrow 2$ scalar scattering states, to be limited to a maximum value of 8π . (A comprehensive examination of unitarity in 3HDMs can be found in [28].)

- **Vacuum Stability:** To maintain the stability of the Higgs potential, it is necessary to ensure that the latter remains bounded from below in all directions in field space. In Ref. [27], the necessary and sufficient conditions to ensure the potential remains positive have been established:

$$\rho_1 > 0, \quad \rho_2 > 0, \quad \rho_\eta > 0, \quad (8)$$

$$\rho_x > -\sqrt{\rho_1\rho_2}, \quad \rho_y > -\sqrt{\rho_1\rho_\eta}, \quad \rho_y > -\sqrt{\rho_2\rho_\eta}, \quad (9)$$

$$\rho_y \geq 0 \vee \left(\rho_\eta\rho_x - \rho_y^2 > -\sqrt{(\rho_\eta\rho_1 - \rho_y^2)(\rho_\eta\rho_2 - \rho_y^2)} \right), \quad (10)$$

where

$$\rho_x = \rho_3 + \min(0, \rho_4 - |\rho_5|), \quad (11)$$

$$\rho_y = \rho_a + \min(0, \rho_b - |\rho_c|). \quad (12)$$

3.2 Experimental Constraints

Experimental constraints provide the most accurate information about the Higgs mass spectrum, whether for the observed one at 125 GeV or companion states possibly existing at the EW scale. In this regard, EW Precision Observables (EWPOs), SM-like Higgs boson measurements, new Higgs boson direct searches as well as flavour observables set limits on the various Higgs boson properties. Below, we summarise the most important constraints.

- **EWPOs:** The precision tests of quantum effects on EW parameters, such as gauge couplings and gauge boson masses, are quite important to check the validity of any new BSM physics. Thus, S , T , and U , the so-called ‘oblique parameters’ [32, 33] that characterise EW radiative corrections, need to be compared to the ensuing I(1+2)HDM predictions. The currently measured values [34] of such observables are:

$$\Delta S = -0.01 \pm 0.07, \quad \Delta T = 0.04 \pm 0.06 \quad \text{and} \quad \rho_{ST} = 0.92 \quad (\text{with } \Delta U = 0), \quad (13)$$

where

$$\Delta X^{\text{I(1+2)HDM}} = \Delta X^{\text{2HDM}} + \Delta X^{\text{IDM}}, \quad X = S, T. \quad (14)$$

The formulae for the 2HDM can be found in Refs. [32, 33, 35] and [36], respectively. In Ref. [28], the authors presented the general expressions for the I(1+2)HDM.

- **SM-like Higgs Boson Discovery:** To ensure the consistency between our parameter space and the experimental measurements of the properties of the discovered SM-like Higgs boson with a mass of approximately 125 GeV, we have utilised the publicly available code `HiggsSignals-3` [37]. This code allows us to evaluate a χ^2 measure, which assesses the compatibility of the Higgs signal strengths observed at the Tevatron and LHC with the predictions of our model. We have selected the I(2+1)HDM parameter space that satisfies the condition $\chi_{125}^2 < 189.42$, corresponding to a Confidence Level (CL) of 95% with 159 degrees of freedom, where χ_{125}^2 represents the value computed by `HiggsSignals-3` for the 125 GeV Higgs signal strength measurements.
- **Non-SM-like Higgs Boson Exclusions:** To ensure that our parameter space remains within the acceptable exclusion limits from new Higgs boson searches carried out at LEP, the Tevatron, and LHC, we have used the publicly available `HiggsBounds-6` [38] module, with default settings.

- **Flavour Constraints:** To test the I(1+2)HDM model against flavour physics constraints, we have used the public C++ SuperIso [39] program, and so several observables have been checked such as: $BR(B \rightarrow X_s \gamma)$ [40], $BR(B_s \rightarrow \mu^+ \mu^-)$ [?, 41, 42], $BR(B \rightarrow \tau \nu)$ [40] and many others.

4 The Excesses in $h \rightarrow \gamma\gamma$, $\tau^+ \tau^-$ and $b\bar{b}$ Channels

Our analysis involves evaluating the signal strengths of the aforementioned excesses within the I(1+2)HDM (we will use the notation NP in formulae to refer to it) using the Narrow Width Approximation (NWA) and examining whether a unified explanation for all these may be achieved. The results of searches for a possible 95 GeV new state, that we denote by ϕ_{95}^{NP} and assume to be CP-even (i.e., a scalar), as mentioned, can be cast in terms of signal strengths relative to the predictions for a SM-like Higgs state of 95 GeV (hereafter, denoted by h_{95}^{SM}) in each of the discussed three channels.

- **Searches in the $b\bar{b}$ channel:**

$$\mu_{b\bar{b}}(\phi_{95}) = \frac{\sigma(e^+e^- \rightarrow Z\phi_{95}^{\text{NP}})\text{BR}(\phi_{95}^{\text{NP}} \rightarrow b\bar{b})}{\sigma(e^+e^- \rightarrow Zh_{95}^{\text{SM}})\text{BR}(h_{95}^{\text{SM}} \rightarrow b\bar{b})} = \left| c_{\phi_{95}^{\text{NP}}ZZ} \right|^2 \times \frac{\text{BR}(\phi_{95}^{\text{NP}} \rightarrow b\bar{b})}{\text{BR}(h_{95}^{\text{SM}} \rightarrow b\bar{b})}. \quad (15)$$

- **Searches in the $\gamma\gamma$ channel:**

$$\mu_{\gamma\gamma}(\phi_{95}) = \frac{\sigma(gg \rightarrow \phi_{95}^{\text{NP}})\text{BR}(\phi_{95}^{\text{NP}} \rightarrow \gamma\gamma)}{\sigma(gg \rightarrow h_{95}^{\text{SM}})\text{BR}(h_{95}^{\text{SM}} \rightarrow \gamma\gamma)} = \left| c_{\phi_{95}^{\text{NP}}t\bar{t}} \right|^2 \times \frac{\text{BR}(\phi_{95}^{\text{NP}} \rightarrow \gamma\gamma)}{\text{BR}(h_{95}^{\text{SM}} \rightarrow \gamma\gamma)}. \quad (16)$$

- **Searches in the $\tau^+ \tau^-$ channel:**

$$\mu_{\tau^+\tau^-}(\phi_{95}) = \frac{\sigma(gg \rightarrow \phi_{95}^{\text{NP}})\text{BR}(\phi_{95}^{\text{NP}} \rightarrow \tau^+\tau^-)}{\sigma(gg \rightarrow h_{95}^{\text{SM}})\text{BR}(h_{95}^{\text{SM}} \rightarrow \tau^+\tau^-)} = \left| c_{\phi_{95}^{\text{NP}}t\bar{t}} \right|^2 \times \frac{\text{BR}(\phi_{95}^{\text{NP}} \rightarrow \tau^+\tau^-)}{\text{BR}(h_{95}^{\text{SM}} \rightarrow \tau^+\tau^-)}. \quad (17)$$

Here, $c_{\phi_{95}^{\text{NP}}ZZ}$ and $c_{\phi_{95}^{\text{NP}}t\bar{t}}$ are the reduced couplings of the ϕ_{95}^{NP} to ZZ and $t\bar{t}$ compared to the SM values, respectively.

With a local significance of 2.3σ and 3.1σ , respectively, at a mass value around 95 GeV, the four LEP Collaborations [43] and CMS [21] have reported the following experimental values for the $b\bar{b}$ and $\tau^+ \tau^-$ signal strengths:

$$\mu_{b\bar{b}}^{\text{LEP}}(\phi_{95}) = 0.117 \pm 0.057 \quad \text{and} \quad \mu_{\tau^+\tau^-}^{\text{CMS}}(\phi_{95}) = 1.2 \pm 0.5, \quad (18)$$

while for the di-photon channel, a local excess of 1.7σ and 2.9σ is reported by both ATLAS [21], $\mu_{\gamma\gamma}^{\text{ATLAS}}(\phi_{95}) = 0.18 \pm 0.1$, and CMS [12], $\mu_{\gamma\gamma}^{\text{CMS}}(\phi_{95}) = 0.33^{+0.19}_{-0.12}$ (with the peak position between 95.3 and 95.4 GeV). Recently, a combined signal strength of the two experimental results in this channel, without possible correlations, was given as [21]

$$\mu_{\gamma\gamma}^{\text{ATLAS+CMS}}(\phi_{95}) = 0.24^{+0.09}_{-0.08}. \quad (19)$$

Consequently, in the following, we examine whether these anomalies can be accommodated within the parameter space of the I(1+2)HDM, focusing our discussion on the Type-I scenario. To do so, a χ^2 analysis is performed for each channel involving the $h \equiv \phi_{95}^{\text{NP}}$ state as follows:

$$\chi_{\gamma\gamma, \tau^+\tau^-, b\bar{b}}^2 = \frac{\left(\mu_{\gamma\gamma, \tau^+\tau^-, b\bar{b}} - \mu_{\gamma\gamma, \tau^+\tau^-, b\bar{b}}^{\text{exp}} \right)^2}{\left(\Delta \mu_{\gamma\gamma, \tau^+\tau^-, b\bar{b}}^{\text{exp}} \right)^2}, \quad (20)$$

where we consider only points that lie within the 95% CL region. However, to make sure that such a sample not only explains the observed excesses but also remains consistent with the well-measured proprieties of h_{125} , we also define

$$\chi^2 = \chi_{125}^2 + \chi_{\gamma\gamma, \tau^+\tau^-, b\bar{b}}^2. \quad (21)$$

5 Results

To perform our numerical analysis, we have implemented the I(1+2)HDM Type-I in a **Fortran** code which allows a fast numerical evaluation of the relevant experimental observables over the theoretical parameter space. The data generated are then tested against the constraints previously discussed, through a **Python** interface. As mentioned, in doing so, the heaviest CP-even Higgs boson, H , is set to mimic the SM-like Higgs boson observed at the LHC, specifically, with a mass of 125.09 GeV. Crucially, the mass of the lightest CP-even Higgs, h , is allowed to vary within the range [94, 97] GeV, where the $\gamma\gamma$ excess is most pronounced (as emphasised in the introduction). The remaining scanned parameters are summarised in Tab. 2.

Parameter	m_h	m_H	m_A	m_{H^\pm}	$\tan\beta$
Scan Range	[94, 97]	125.09	[100, 10 ³]	[90, 10 ³]	[0.5, 50]
Parameter	$\sin(\beta - \alpha)$	m_{12}^2	$m_\chi, m_{\chi_\alpha}, m_{\chi^\pm}$	λ_η	m_η^2
Scan Range	[-0.4, 0.5]	[-10 ³ , 10 ³]	[90, 10 ³]	[7, 12]	[-10 ⁵ , 10 ⁵]

Table 2: Scan ranges of the I(1+2)HDM Type-I parameters. (Mass (squared) are in GeV⁽²⁾.)

All excesses are then evaluated simultaneously using a χ^2 test, requiring $\chi_{\gamma\gamma+\tau^+\tau^-+b\bar{b}}^2 \leq 8.03$ at the 2σ CL to ensure compatibility with data. We anticipate here that our results will point towards the possible existence of a light CP-even (or scalar) Higgs boson, supporting our exploration of the I(1+2)HDM Type-I. These will be mapped in the forthcoming plots in terms of two-dimensional planes of the signal strength parameters: $(\mu_{bb} - \mu_{\gamma\gamma})$, $(\mu_{\tau^+\tau^-} - \mu_{\gamma\gamma})$ and $(\mu_{\tau^+\tau^-} - \mu_{bb})$, thereby providing insights into parameter correlations and the overall model fit.

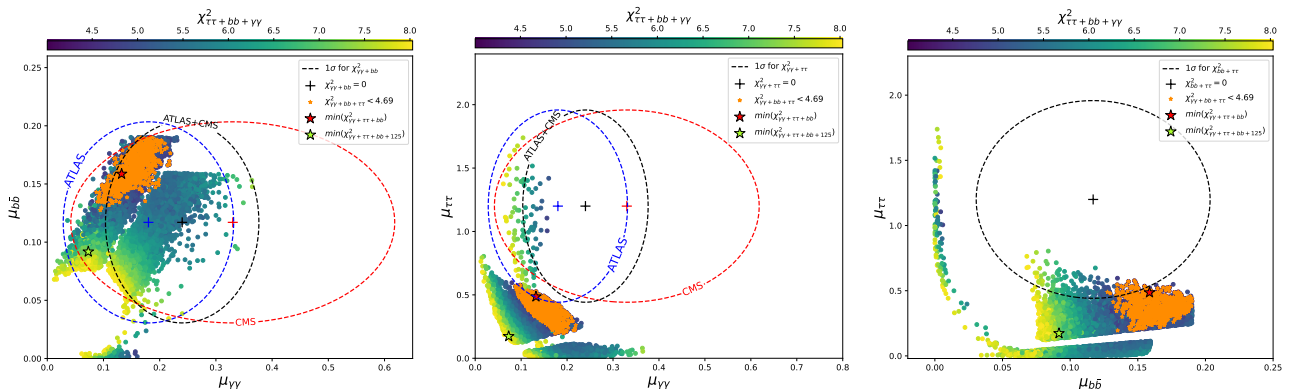


Figure 1: Correlations among the signal strengths in Eqs. (15)–(17), with the $\chi_{\gamma\gamma+\tau^+\tau^-+b\bar{b}}^2$ value represented by the colour bar and the $\min(\chi_{\gamma\gamma+\tau^+\tau^-+b\bar{b}}^2)$ best-fit point marked by a red star. The ATLAS and CMS results, along with their corresponding 1σ bands, are also depicted through the ellipse contours, which indicate the regions corresponding to the excess observed at such a CL. (We use the $\chi_x^2 + \chi_y^2 = 2.30$ relation, where the indexes x and y represent each possible pair of the three signal channels: $\gamma\gamma$, $\tau^+\tau^-$ and $b\bar{b}$.)

Fig. 1 displays the results for our fits as a colour map, projected onto the signal strength planes $(\mu_{\gamma\gamma} - \mu_{bb})$ (left), $(\mu_{\gamma\gamma} - \mu_{\tau^+\tau^-})$ (middle) and $(\mu_{bb} - \mu_{\tau^+\tau^-})$ (right), following our scan of I(1+2)HDM Type-I parameter space. The black cross corresponds to $\chi^2_{x,y} = 0$ (for all combinations of $x, y = \gamma\gamma, \tau^+\tau^-, b\bar{b}$) whereas the green and red stars mark the points of $\min(\chi^2_{\gamma\gamma+\tau^+\tau^-+b\bar{b}+125})$ and $\min(\chi^2_{\gamma\gamma+\tau^+\tau^-+b\bar{b}})$, representing the best-fit point with and without including the SM-like Higgs data in the fit, respectively. The left panel reveals a weak correlation between $\mu_{\gamma\gamma}$ and μ_{bb} , with most allowed points clustering around $\mu_{bb} \sim 0.1$ and $\mu_{\gamma\gamma} \sim 0.2 - 0.3$, altogether appearing quite consistent with experimental data. In contrast, regarding the $\mu_{\tau^+\tau^-}$ excess, a broader range of values is permitted as can be seen from the middle panel, reflecting the looser experimental constraints in the $\tau^+\tau^-$ channel. It is straightforward to see, from both plots, how the combined 1σ contour encompasses the χ^2 minima, consistent with a potential light Higgs boson interpretation. The situation does not change substantially in the right panel, where a positive correlation between $\mu_{b\bar{b}}$ and $\mu_{\tau^+\tau^-}$ is highlighted, forming a narrow band where $\mu_{\tau^+\tau^-}$ remains relatively small (< 0.2).

Still in Fig. 1, for guiding further investigations, we exhibit with an orange colour the data samples corresponding to $\chi^2_{\gamma\gamma+\tau^+\tau^-+b\bar{b}} \leq 4.69$. As it can be seen from Fig. 1, this description of the three observables at 1.3σ CL provide a quantitative measure of how well the model simultaneously fits all the observed excesses, most notably in the $(\mu_{\gamma\gamma} - \mu_{bb})$ plane. We add here that the red star, corresponding to $\min(\chi^2_{\gamma\gamma+\tau^+\tau^-+b\bar{b}}) = 3.94$, represents the best-fit point at approximately 1.04σ CL, providing the best configuration of the I(1+2)HDM Type-I in explaining all the experimental anomalies.

Again, in relation to Fig. 1, we further notice here that the inert charged states χ^\pm play a crucial role in $\mu_{\gamma\gamma}$ and, consequently, all other observables. Specifically, the decay $h \rightarrow \gamma\gamma$ is mediated at one-loop level by the virtual exchange of χ^\pm , in addition to the 2HDM-like contribution generated by H^\pm and the SM contribution dominated by the W and top loops. The corresponding decay width is given explicitly by

$$\Gamma(h \rightarrow \gamma\gamma) = \frac{G_F \alpha^2 m_h^3}{128\sqrt{2}\pi^3} \left| \sum_f \underbrace{Q_f^2 N_c \eta_{hff} A_{\frac{1}{2}}^{\gamma\gamma}(\tau_f)}_{C_{\text{top}}} + \underbrace{\eta_{hWW} A_1^{\gamma\gamma}(\tau_W)}_{C_W} - \underbrace{\frac{m_W}{g m_{H^\pm}^2} \eta_{hH^\pm H^\mp} A_0^{\gamma\gamma}(\tau_{H^\pm})}_{C_{H^\pm}} - \underbrace{\frac{m_W}{g m_{\chi^\pm}^2} \eta_{h\chi^\pm \chi^\mp} A_0^{\gamma\gamma}(\tau_{\chi^\pm})}_{C_{\chi^\pm}} \right|^2. \quad (22)$$

Here, N_c represents the colour factor, with $N_c = 3$ for quarks and $N_c = 1$ for leptons, while Q_f denotes the electric charge of a particle in the loop. The fine-structure constant is denoted by α , while $A_{1/2}^{\gamma\gamma}$, A_1^{VV} , and $A_0^{\gamma\gamma}$ are the form factors associated with: spin-1/2 fermions (f), W -boson and charged scalars (H^\pm and χ^\pm), respectively. Such dimensionless functions characterise the contributions of each particle and can be expressed in terms of Passarino-Veltman functions [44].

Clearly, the former contribution depends on the scalar mass m_{χ^\pm} and reduced trilinear coupling $h\chi^+\chi^-$. This latter reads as

$$\tilde{c}_{h\chi^+\chi^-} = -\frac{1}{g} \frac{m_W}{m_{\chi^\pm}^2} c_{h1\chi^+\chi^-} \quad \text{where} \quad c_{h\chi^+\chi^-} = -\lambda_a v \sin(\beta - \alpha), \quad (23)$$

according to which substantial constructive interference between the χ^\pm and H^\pm loops may occur, for non-vanishing $\sin(\beta - \alpha)$.

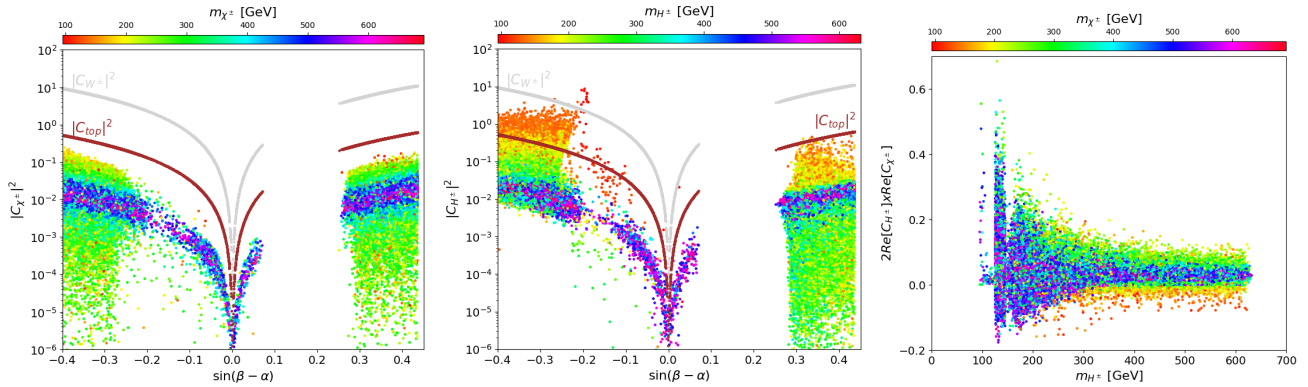


Figure 2: The squared moduli C_{χ^\pm} (left), C_{H^\pm} (middle) and their interference (right) for $h \rightarrow \gamma\gamma$ amplitude, as a function of either $\sin(\beta - \alpha)$ or m_{H^\pm} . The modified top and W^\pm contributions are also shown for comparison. The colour coding exhibits the charged scalar boson masses m_{χ^\pm} and m_{H^\pm} .

To highlight the effect of the inert charged scalars on such a decay width, and thus on the $\mu_{\gamma\gamma}$ excess, we display in Fig. 2 the squared moduli $|C_{\chi^\pm}|^2$ and $|C_{H^\pm}|^2$, along with their interference $2 \times \Re(C_{\chi^\pm}) \times \Re(C_{H^\pm})$, as a function of m_{χ^\pm} , m_{H^\pm} and $\sin(\beta - \alpha)$. From the left panel, it is evident that the inert charged contribution is non-negligible and could contribute significantly for $|\sin(\beta - \alpha)| \gtrsim 0.3$ and $m_{\chi^\pm} \lesssim 300$ GeV but remains below the $|C_{\text{top}}|^2$ term over the allowed space parameter. The charged Higgs boson H^\pm , meanwhile, has a key role in enhancing or suppressing the $h \rightarrow \gamma\gamma$ partial width. In fact, for $|\sin(\beta - \alpha)| \gtrsim 0.3$ together with a light-charged scalar boson mass (below 180 GeV), one can see that $|C_{H^\pm}|^2$ term can surpass the $|C_{\text{top}}|^2$ one and even exceed $|C_{W^\pm}|^2$ for $m_{H^\pm} \approx 123$ GeV (middle panel). However, despite being less dominant, the χ^\pm loops could constructively interfere with the H^\pm ones, reaching a maximum for $m_{H^\pm} \approx 128.87$ GeV, $m_{\chi^\pm} \approx 233.96$ GeV and $\sin(\beta - \alpha) \approx -0.35$, as depicted in the right plot of Fig. 2.

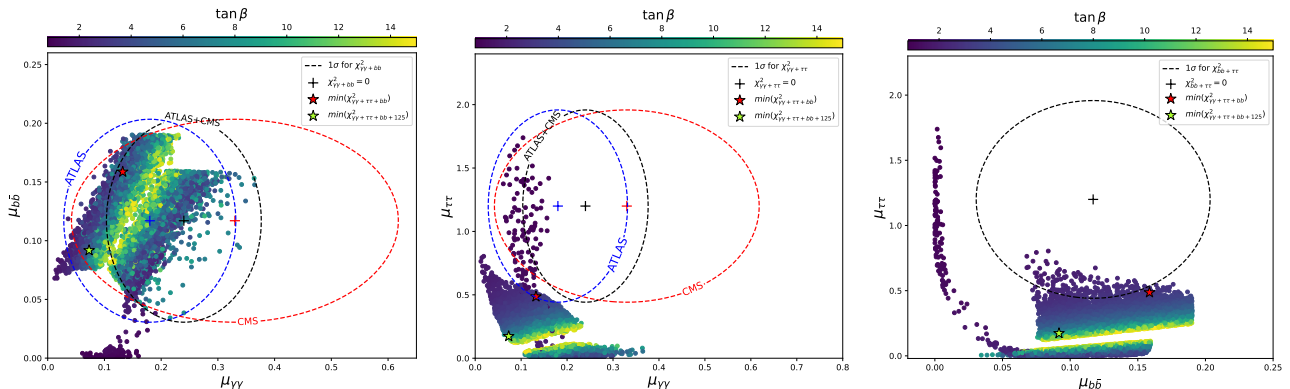


Figure 3: Correlations among the signal strengths $(\mu_{bb} - \mu_{\gamma\gamma})$, $(\mu_{\tau+\tau^-} - \mu_{\gamma\gamma})$ and $(\mu_{\tau+\tau^-} - \mu_{bb})$, with the $\tan\beta$ value represented by the colour bar and the $\min(\chi^2_{\gamma\gamma+\tau+\tau^-+bb})$ best-fit point marked by a red star. The ATLAS and CMS results, as described in the previous figure, are also included.

Another phenomenologically interesting quantity to study is $\tan\beta$, which influences nearly all the Higgs couplings. So, by considering the ATLAS and CMS results, along with their corresponding 1σ uncertainties, we investigate the constraining power of each correlation on $\tan\beta$. This behaviour is exhibited in Fig. 3. A striking observation from the left plot of Fig. 3 is that many points fall within the 1σ ellipse, indicating that both the μ_{bb} excess and the $\mu_{\gamma\gamma}$ one can be simultaneously fit without favouring any specific value of $\tan\beta$, indeed allowing for a broad range of it, i.e., $0.8 \leq \tan\beta \leq 14$. This is in turn supported by the position, within the

1σ contour, of the best-fit point (marked by the green star) that minimise $\chi^2_{\gamma\gamma+\tau^+\tau^-+b\bar{b}+125}$. In contrast, $\mu_{\tau^+\tau^-}$ correlates (purple points) with either $\mu_{\gamma\gamma}$ or $\mu_{b\bar{b}}$ in such a way that only low values of $\tan\beta$ are viable, as reflected by the middle and right plots in Fig. 3. Altogether, combining all excesses, one can set the upper bound $\tan\beta \leq 5$, providing valuable insights into the viable parameter space configurations of the I(1+2)HDM Type-I.

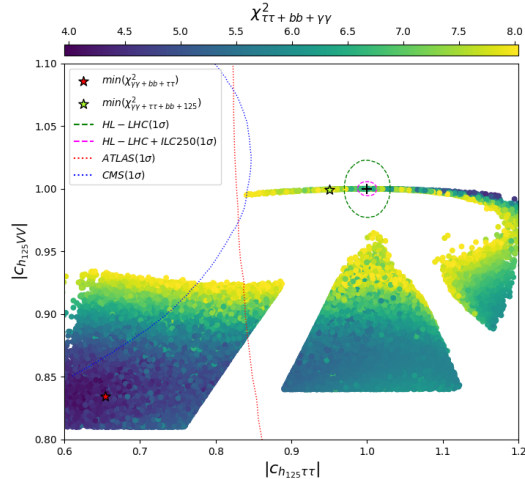


Figure 4: Scattered points in the plane ($|c_{h_{125}\tau^+\tau^-}|$, $|c_{h_{125}VV}|$) following our scan, with the colour bar indicating the combined value of χ^2 for the three discussed excesses. Projections from the HL-LHC and an ILC running at 250 GeV are also sketched.

Since the coupling of the SM-like Higgs boson to gauge bosons is extremely constraining for BSM scenarios (through mixing), the measurement of this quantity could afford one with some understanding of the observed excesses at 95 GeV. In this connection, we display in Fig. 4 the $\chi^2_{\gamma\gamma+\tau^+\tau^-+b\bar{b}}$ distribution obtained from our parameter scan as a function of $|c_{h_{125}\tau^+\tau^-}|$ and $|c_{h_{125}VV}|$, the values of the $h_{125}^{\text{SM}}\tau^+\tau^-$ and $h_{125}^{\text{SM}}VV$ ($V = W^\pm, Z$) couplings (in modulus), respectively, in the I(1+2)HDM Type-I. The dotted red and blue lines represent the current 1σ uncertainties for the experimental measured values of these two coupling coefficients while the magenta and green ellipses indicate the projected uncertainties achievable at the High-Luminosity LHC (HL-LHC) [?, 45] (with 3 ab^{-1} of integrated luminosity) and a possible International Linear Collider (ILC) running at a center-of-mass energy of 250 GeV [46] (with 1 ab^{-1} of integrated luminosity). The SM prediction for both coupling coefficients is marked by a “+”.

The data sample here fulfills both $\chi^2_{\gamma\gamma+\tau^+\tau^-+b\bar{b}} \leq 8.03$ and $\chi^2_{125} \leq 189.42$, with the results from the I(1+2)HDM Type-I showing that most points are concentrated at low values, well below unity for both $|c_{h_{125}\tau^+\tau^-}|$ and $|c_{h_{125}VV}|$. This is related to the fact that the minimum of $\chi^2_{\gamma\gamma+\tau^+\tau^-+b\bar{b}}$ (red star) requires a non-vanishing value of $\sin(\beta - \alpha)$ (so that the χ^\pm contribution cooperates with the H^\pm one in $h \rightarrow \gamma\gamma$, as previously explained), hence, $|c_{h_{125}VV}| = |\cos(\beta - \alpha)| < 1$. Only a tiny portion of this BSM parameter space is potentially compatible with HL-LHC and ILC (projected) measurements (assuming the same central values of $|c_{h_{125}\tau^+\tau^-}|$ and $|c_{h_{125}VV}|$ as presently), so that either of these machines will prove a crucial testing ground of the viability of our model (assuming persistence of the current $\gamma\gamma$, $b\bar{b}$ and $\tau^+\tau^-$ excesses at the current level by the end of the LHC runs).

Finally, as intimated, we dwell in some more detail into the $\gamma\gamma$ excess, by presenting in Fig. 5 a superposition of our allowed parameter points and experimental results, by overlaying the former on the combined ATLAS and CMS low mass $\gamma\gamma$ analysis data at 13 TeV, with integrated

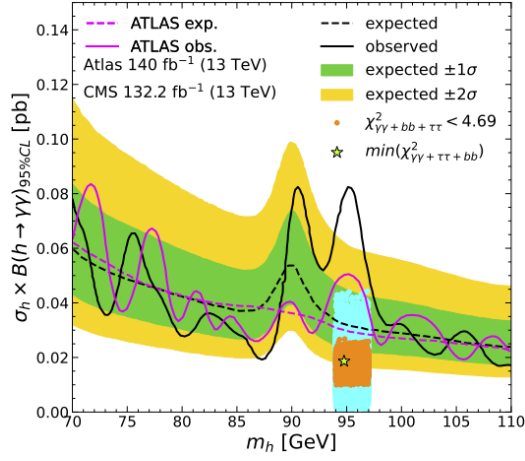


Figure 5: Scattered points in the $[m_h, \sigma_h \times \text{BR}(h \rightarrow \gamma\gamma)]$ plane. The solid and dashed lines indicate the expected and observed cross section limits obtained by ATLAS and CMS, respectively. ATLAS is depicted in magenta, while CMS is shown in black. The green and yellow bands represent the 1σ and 2σ uncertainty intervals, respectively. The orange points feature $\chi^2_{\gamma\gamma+\tau^+\tau^-+b\bar{b}} \leq 4.69$ and describe the excesses at the level of 1.3σ or better, whereas the red points represent $\chi^2_{\gamma\gamma+\tau^+\tau^-+b\bar{b}} > 4.69$ and the $\min(\chi^2_{\gamma\gamma+\tau^+\tau^-+b\bar{b}})$ best-fit point is marked by a green star.

luminosities of 140 fb^{-1} and 132.2 fb^{-1} [10, 47]. The expected and observed ATLAS limits on the cross section times Branching Ratio (BR), i.e., $\sigma(pp \rightarrow h) \times \text{BR}(h \rightarrow \gamma\gamma)$, are indicated by the magenta dashed and solid lines, respectively. The 1σ and 2σ uncertainty bands, resulting from the combined result, are shown in green and yellow, respectively. Superposed on these results, the combined (between ATLAS and CMS) expected and observed limits are illustrated by the black dashed and solid lines, respectively. Altogether, the plot clearly indicates that our parameter points are not only in very good agreement with the LHC excess in the di-photon channel but also that our sample matches well all current anomalous data, as emphasised by the position of the best-fit point explaining the three excesses simultaneously. To summarise the previous results, the details of our best-fit point are presented in Tab. 3.

Parameters	m_h	m_H	m_A	m_{H^\pm}	$\tan\beta$	$\sin(\beta - \alpha)$	m_{12}^2	m_χ	m_{χ_a}	m_{χ^\pm}	λ_η	m_η^2
	94.768	125.09	408.76	436.04	3.89	0.40	914.18	282.79	527.18	336.21	10.19	-88684.35
Signal strengths				$\mu_{\gamma\gamma}$			$\mu_{\tau^+\tau^-}$				$\mu_{b\bar{b}}$	
				0.162			0.412				0.165	

Table 3: Details of the best-fit point corresponding to $\min(\chi^2_{\gamma\gamma+\tau^+\tau^-+b\bar{b}}) = 3.95$. (Mass (squared) are in $\text{GeV}^{(2)}$.)

Furthermore, it is worth mentioning that the I(1+2)HDM Type-I is not only able to explain the current excesses but also has the potential to give distinctive signals at future accelerators, such as an e^+e^- collider. Our findings in Tab. 4 demonstrate that such a machine will have the capability to probe this new state through various production mechanisms, primarily Higgs-strahlung and Vector Boson Fusion (VBF) processes. Indeed, at $\sqrt{s} = 250 \text{ GeV}$, the $e^+e^- \rightarrow Z^* \rightarrow Zh_{95}$ process dominates with a sizable cross section of 55.5 fb , making it the most promising channel for future discovery. As the center-of-mass-energy increases, the VBF channels become increasingly more relevant, with $\sigma(e^+e^- \rightarrow \nu_e \bar{\nu}_e h_{95})$ reaching 15.01 fb at $\sqrt{s} = 500 \text{ GeV}$. Similarly,

the $e^+e^- \rightarrow e^+e^-h_{95}$ process exhibits a steady rise, reaching nearly 1 fb at 500 GeV. These cross sections indicate that future e^+e^- colliders would provide a powerful testing ground for the I(1+2)HDM Type-I, by enabling precise measurements of the properties of the observed 95 GeV scalar state.

$\sqrt{s} =$	250 GeV	350 GeV	500 GeV
$\sigma(e^+e^- \rightarrow Zh_{95})$	55.5 fb	23.32 fb	9.58 fb
$\sigma(e^+e^- \rightarrow \nu_e\bar{\nu}_e h_{95})$	2.645 fb	7.269 fb	15.01 fb
$\sigma(e^+e^- \rightarrow e^+e^-h_{95})$	0.212 fb	0.557 fb	0.983 fb

Table 4: Cross sections for Higgs-strahlung, W^+W^- - and Z-fusion processes for h_{95} at the three centre-of-mass energies corresponding to the best-fit point $\min(\chi^2_{\gamma\gamma+\tau^+\tau^-+b\bar{b}}) = 3.95$.

6 Conclusions

In summary, we have looked at how to address the $\gamma\gamma$, $b\bar{b}$ and $\tau^+\tau^-$ excesses observed around 95 GeV by the LHC and LEP, within the I(1+2)HDM Type-I, while remaining consistent with measured properties of the Higgs boson observed at 125 GeV as well as other theoretical and experimental constraints. Rigorous data evaluations, complemented by detailed simulations and advanced computational methods, have been carried out, followed by a study of the correlations between the signal strengths $\mu_{\gamma\gamma}$, $\mu_{b\bar{b}}$ and $\mu_{\tau^+\tau^-}$ at the 1σ CL.

Our findings suggest that all two-dimensional correlations, i.e, on the planes $(\mu_x-\mu_y)$, with $x, y = \gamma\gamma, b\bar{b}, \tau^+\tau^-$, incorporate many points lying entirely within the 1σ CL, indicating that our model can simultaneously explain all three excesses, particularly for low values of $\tan\beta$. Besides, our study indicates there is a crucial distinction compared to results found in [25], wherein the 2HDM Type-I was found to struggle in accommodating all three excesses simultaneously within a viable parameter space so that embedding an extra inert doublet significantly enhances the theory compatibility with data.

However, as the LHC has not yet completed its Run 3, extended data collection will provide a valuable opportunity to further investigate the excesses observed around 95 GeV and also to clarify the interplay between the coupling measurements of the h_{95}^{NP} (the h state of our BSM scenario) and h_{125}^{SM} (the H state of our BSM scenario), which will be crucial in assertion or not of such new physics. However, we have also demonstrated that, if the level of confidence of these three excesses remains so at the end of the LHC era, both the HL-LHC and ILC will be able to finally access the viability of the I(1+2)HDM Type-I as the underlying BSM scenario, by either exploiting further the excesses associated to the h_{95}^{NP} state or else by ever more precise measurements of the h_{125}^{SM} state.

Finally, we have shown that any future e^+e^- collider running at approximately 250, 350, and 500 GeV will have a strong sensitivity to the best-fit point of our model to the current anomalies at 95 GeV, by exploiting the direct production of the h_{95}^{NP} state in both Higgs-strahlung and VBF.

Acknowledgments

SM is supported in part through the NExT Institute and STFC Consolidated Grant ST/X000583/1. AH and LR would like to thank EL-said Ghourmin for his invaluable discussions.

References

- [1] **ATLAS** collaboration, *Observation of a new particle in the search for the Standard Model Higgs boson with the ATLAS detector at the LHC*, *Phys. Lett. B* **716** (2012) 1 [[1207.7214](#)].
- [2] **CMS** collaboration, *Observation of a New Boson at a Mass of 125 GeV with the CMS Experiment at the LHC*, *Phys. Lett. B* **716** (2012) 30 [[1207.7235](#)].
- [3] **Belle** collaboration, *Precise determination of the CKM matrix element $|V_{cb}|$ with $\bar{B}^0 \rightarrow D^{*+} \ell^- \bar{\nu}_\ell$ decays with hadronic tagging at Belle*, [1702.01521](#).
- [4] C. Bobeth, M. Bordone, N. Gubernari, M. Jung and D. van Dyk, *Lepton-flavour non-universality of $\bar{B} \rightarrow D^* \ell \bar{\nu}$ angular distributions in and beyond the Standard Model*, *Eur. Phys. J. C* **81** (2021) 984 [[2104.02094](#)].
- [5] **Muon g-2** collaboration, *Measurement of the Positive Muon Anomalous Magnetic Moment to 0.46 ppm*, *Phys. Rev. Lett.* **126** (2021) 141801 [[2104.03281](#)].
- [6] N. Kurinsky, D. Baxter, Y. Kahn and G. Krnjaic, *Dark matter interpretation of excesses in multiple direct detection experiments*, *Phys. Rev. D* **102** (2020) 015017 [[2002.06937](#)].
- [7] M. Heikinheimo, S. Sassi, K. Nordlund, K. Tuominen and N. Mirabolfathi, *Identification of the low-energy excess in dark matter searches with crystal defects*, *Phys. Rev. D* **106** (2022) 083009 [[2112.14495](#)].
- [8] **ALEPH, DELPHI, L3, OPAL, LEP Working Group for Higgs Boson Searches** collaboration, *Search for neutral MSSM Higgs bosons at LEP*, *Eur. Phys. J. C* **47** (2006) 547 [[hep-ex/0602042](#)].
- [9] **CMS** collaboration, *Search for a standard model-like Higgs boson in the mass range between 70 and 110 GeV in the diphoton final state in proton-proton collisions at $\sqrt{s} = 8$ and 13 TeV*, *Phys. Lett. B* **793** (2019) 320 [[1811.08459](#)].
- [10] **CMS** collaboration, *Search for a standard model-like Higgs boson in the mass range between 70 and 110 GeV in the diphoton final state in proton-proton collisions at $\sqrt{s} = 13$ TeV*, *CMS-PAS-HIG-20-002* (2023) .
- [11] **ATLAS** collaboration, *Search for diphoton resonances in the 66 to 110 GeV mass range using 140 fb^{-1} of 13 TeV pp collisions collected with the ATLAS detector*, .
- [12] **CMS** collaboration.
- [13] G. Cacciapaglia, A. Deandrea, S. Gascon-Shotkin, S. Le Corre, M. Lethuillier and J. Tao, *Search for a lighter Higgs boson in Two Higgs Doublet Models*, *JHEP* **12** (2016) 068 [[1607.08653](#)].

- [14] R. Benbrik, M. Boukidi, S. Moretti and S. Semlali, *Explaining the 96 GeV Di-photon anomaly in a generic 2HDM Type-III*, *Phys. Lett. B* **832** (2022) 137245 [[2204.07470](#)].
- [15] R. Benbrik, M. Boukidi, S. Moretti and S. Semlali, *Probing a 96 GeV Higgs Boson in the Di-Photon Channel at the LHC*, *PoS ICHEP2022* (2022) 547 [[2211.11140](#)].
- [16] D. Azevedo, T. Biekötter and P.M. Ferreira, *2HDM interpretations of the CMS diphoton excess at 95 GeV*, [2305.19716](#).
- [17] T. Biekötter, M. Chakraborti and S. Heinemeyer, *A 96 GeV Higgs boson in the N2HDM*, *Eur. Phys. J. C* **80** (2020) 2 [[1903.11661](#)].
- [18] S. Heinemeyer, C. Li, F. Lika, G. Moortgat-Pick and S. Paasch, *Phenomenology of a 96 GeV Higgs boson in the 2HDM with an additional singlet*, *Phys. Rev. D* **106** (2022) 075003 [[2112.11958](#)].
- [19] T. Biekötter, S. Heinemeyer and G. Weiglein, *Mounting evidence for a 95 GeV Higgs boson*, *JHEP* **08** (2022) 201 [[2203.13180](#)].
- [20] T. Biekötter, S. Heinemeyer and G. Weiglein, *The CMS di-photon excess at 95 GeV in view of the LHC Run 2 results*, [2303.12018](#).
- [21] T. Biekötter, S. Heinemeyer and G. Weiglein, *95.4 GeV diphoton excess at ATLAS and CMS*, *Phys. Rev. D* **109** (2024) 035005 [[2306.03889](#)].
- [22] J. Cao, X. Jia, Y. Yue, H. Zhou and P. Zhu, *96 GeV diphoton excess in seesaw extensions of the natural NMSSM*, *Phys. Rev. D* **101** (2020) 055008 [[1908.07206](#)].
- [23] T. Biekötter, A. Grohsjean, S. Heinemeyer, C. Schwanenberger and G. Weiglein, *Possible indications for new Higgs bosons in the reach of the LHC: N2HDM and NMSSM interpretations*, *Eur. Phys. J. C* **82** (2022) 178 [[2109.01128](#)].
- [24] R. Benbrik, M. Boukidi and S. Moretti, *Superposition of CP-even and CP-odd Higgs resonances: Explaining the 95 GeV excesses within a two-Higgs-doublet model*, *Phys. Rev. D* **110** (2024) 115030 [[2405.02899](#)].
- [25] A. Khanna, S. Moretti and A. Sarkar, *Explaining 95 (or so) GeV Anomalies in the 2-Higgs Doublet Model Type-I*, [2409.02587](#).
- [26] V. Keus, S.F. King and S. Moretti, *Three-Higgs-doublet models: symmetries, potentials and Higgs boson masses*, *JHEP* **01** (2014) 052 [[1310.8253](#)].
- [27] B. Grzadkowski, O.M. Ogreid and P. Osland, *Natural Multi-Higgs Model with Dark Matter and CP Violation*, *Phys. Rev. D* **80** (2009) 055013 [[0904.2173](#)].
- [28] S. Moretti and K. Yagyu, *Constraints on Parameter Space from Perturbative Unitarity in Models with Three Scalar Doublets*, *Phys. Rev. D* **91** (2015) 055022 [[1501.06544](#)].
- [29] S.L. Glashow and S. Weinberg, *Natural Conservation Laws for Neutral Currents*, *Phys. Rev. D* **15** (1977) 1958.
- [30] G.C. Branco, P.M. Ferreira, L. Lavoura, M.N. Rebelo, M. Sher and J.P. Silva, *Theory and phenomenology of two-Higgs-doublet models*, *Phys. Rept.* **516** (2012) 1 [[1106.0034](#)].
- [31] J.F. Gunion and H.E. Haber, *The CP conserving two Higgs doublet model: The Approach to the decoupling limit*, *Phys. Rev. D* **67** (2003) 075019 [[hep-ph/0207010](#)].

- [32] M.E. Peskin and T. Takeuchi, *Estimation of oblique electroweak corrections*, *Phys. Rev. D* **46** (1992) 381.
- [33] W. Grimus, L. Lavoura, O.M. Ogreid and P. Osland, *The Oblique parameters in multi-Higgs-doublet models*, *Nucl. Phys. B* **801** (2008) 81 [0802.4353].
- [34] **Particle Data Group** collaboration, *Review of Particle Physics*, *PTEP* **2020** (2020) 083C01.
- [35] W. Grimus, L. Lavoura, O.M. Ogreid and P. Osland, *A Precision constraint on multi-Higgs-doublet models*, *J. Phys. G* **35** (2008) 075001 [0711.4022].
- [36] R. Barbieri, L.J. Hall and V.S. Rychkov, *Improved naturalness with a heavy Higgs: An Alternative road to LHC physics*, *Phys. Rev. D* **74** (2006) 015007 [hep-ph/0603188].
- [37] P. Bechtle, S. Heinemeyer, T. Klingl, T. Stefaniak, G. Weiglein and J. Wittbrodt, *HiggsSignals-2: Probing new physics with precision Higgs measurements in the LHC 13 TeV era*, *Eur. Phys. J. C* **81** (2021) 145 [2012.09197].
- [38] P. Bechtle, D. Dercks, S. Heinemeyer, T. Klingl, T. Stefaniak, G. Weiglein et al., *HiggsBounds-5: Testing Higgs Sectors in the LHC 13 TeV Era*, *Eur. Phys. J. C* **80** (2020) 1211 [2006.06007].
- [39] F. Mahmoudi, *SuperIso v2.3: A Program for calculating flavor physics observables in Supersymmetry*, *Comput. Phys. Commun.* **180** (2009) 1579 [0808.3144].
- [40] **HFLAV** collaboration, *Averages of b-hadron, c-hadron, and τ -lepton properties as of summer 2016*, *Eur. Phys. J. C* **77** (2017) 895 [1612.07233].
- [41] **LHCb** collaboration, *Measurement of the $B_s^0 \rightarrow \mu^+ \mu^-$ decay properties and search for the $B^0 \rightarrow \mu^+ \mu^-$ and $B_s^0 \rightarrow \mu^+ \mu^- \gamma$ decays*, *Phys. Rev. D* **105** (2022) 012010 [2108.09283].
- [42] **LHCb** collaboration, *Analysis of Neutral B-Meson Decays into Two Muons*, *Phys. Rev. Lett.* **128** (2022) 041801 [2108.09284].
- [43] **LEP Working Group for Higgs boson searches, ALEPH, DELPHI, L3, OPAL** collaboration, *Search for the standard model Higgs boson at LEP*, *Phys. Lett. B* **565** (2003) 61 [hep-ex/0306033].
- [44] G. Passarino and M.J.G. Veltman, *One Loop Corrections for $e^+ e^-$ Annihilation Into $\mu^+ \mu^-$ in the Weinberg Model*, *Nucl. Phys. B* **160** (1979) 151.
- [45] M. Cepeda et al., *Report from Working Group 2: Higgs Physics at the HL-LHC and HE-LHC*, *CERN Yellow Rep. Monogr.* **7** (2019) 221 [1902.00134].
- [46] P. Bambade et al., *The International Linear Collider: A Global Project*, 1903.01629.
- [47] C. Arcangeletti. on behalf of ATLAS collaboration, LHC Seminar https://indico.cern.ch/event/1281604/attachments/2660420/4608571/LHCseminarArcangeletti_final.pdf, 7th of June, 2023.